Composites Part B 158 (2019) 259–268

Contents lists available at ScienceDirect

Composites Part B

journal homepage: www.elsevier.com/locate/compositesb

Interfacially reinforced carbon fiber/epoxy composite laminates via in-situ synthesized graphitic carbon nitride (g-C_3N_4)

Bo Song[a,b,*], Tingting Wang[b], Li Wang[b], Hu Liu[c,d], Xianmin Mai[e,***], Xiaojing Wang[c,f], Ning Wang[g], Yudong Huang[h], Yong Ma[c,i,**], Yang Lu[j], Evan K. Wujcik[j], Zhanhu Guo[c,****]

[a] Marine College, Shandong University, Weihai, Shandong, 264209, China
[b] School of Mechanical, Electrical & Information Engineering, Shandong University, Weihai, Shandong, 264209, China
[c] Integrated Composites Laboratory (ICL), Department of Chemical & Biomolecular Engineering, University of Tennessee, Knoxville, TN, 37996, USA
[d] Key Laboratory of Materials Processing and Mold (Zhengzhou University), Ministry of Education, National Engineering Research Center for Advanced Polymer Processing Technology, Zhengzhou University, Zhengzhou, 450002, China
[e] School of Urban Planning and Architecture, Southwest Minzu University, Chengdu, 610041, China
[f] School of Material Science and Engineering, Jiangsu University of Science and Technology, Zhenjiang, Jiangsu, 212003, China
[g] State Key Laboratory of Marine Resource Utilization in South China Sea, Hainan University, Haikou, 570228, China
[h] School of Chemistry and Chemical Engineering, Harbin Institute of Technology, Harbin, Helongjiang, 150001, China
[i] School of Materials Science and Engineering, Shandong University of Science and Technology, Qingdao, 266590, China
[j] Materials Engineering and Nanosensor [MEAN] Laboratory, Department of Chemical and Biological Engineering, The University of Alabama, Tuscaloosa, USA

ARTICLE INFO

Keywords:
Carbon fibers
Polymer-matrix composites (PMCs)
Fiber/matrix bond
Interphase/interface
Laminate mechanics

ABSTRACT

Carbon fiber composite laminates were interfacially reinforced through in-situ synthesis of g-C_3N_4 on the carbon fibers. The introduced g-C_3N_4 greatly improved the roughness, functional groups and wettability on the carbon fiber surface and markedly enhanced the interfacial properties of composite laminates. The surface free energy of carbon fibers was increased by 67.81%. Interlaminar shear strength and interfacial shear strength of composite laminates were increased from 51.84 to 72.09 MPa and 44.62–73.41 MPa, respectively. The significantly enhanced interfacial properties enabled the mechanical performance of composite laminates to reach a superior state. Tensile strength and bending strength were increased by 19.54 and 10.51%, respectively. The total absorbed energy of impact experiment was also enhanced from 1.14 to 1.78 J. Meanwhile, dynamic mechanical properties and hydrothermal aging resistance were also ameliorated significantly. The improved interfacial properties and mechanical properties were ascribed to the increased mechanical interlocking, enhanced chemical bonding and ameliorated wettability created by g-C_3N_4.

1. Introduction

Carbon fiber reinforced epoxy composites (CFRECs) as ideal structural materials with the merit of high strength-to-weight ratio and rigidity have now been widely used in aerospace, civil engineering, automotive, sports goods and other field [1–3]. In general, the ultimate performance of composites is largely dependent on reinforcement, matrix and interphase [4–7]. Interphase as a “bridge” of bonding and load transfer between carbon fiber (CF) and epoxy resin has a crucial influence on the ultimate performance of CFRECs [8–12]. However, the poor interfacial compatibility between CF and epoxy resin results in low interfacial strength and impact toughness, which severely limit further development and applications of CFRECs [13–18]. For the past thirty years, considerable research efforts have been made to improve the interfacial compatibility between CF and epoxy resin. Constructing interphase containing nanomaterials is considered as an effective method to solve this problem [19–22]. Various strategy have been employed to create interphase containing nanomaterials, such as coating with sizing agent [23–27], in-situ synthesis [28–30], chemical grafting [31–33] and electrochemical deposition (ECD) [34–37]. Among those

* Corresponding author. Marine College, Shandong University, Weihai, Shandong, 264209, China.
** Corresponding author. School of Materials Science and Engineering, Shandong University of Science and Technology, Qingdao, 266590, China.
*** Corresponding author. School of Urban Planning and Architecture, Southwest Minzu University, Chengdu, 610041, China.
**** Corresponding author. Integrated Composites Laboratory (ICL), Department of Chemical & Biomolecular Engineering, University of Tennessee, Knoxville, TN, 37996, USA.
E-mail addresses: songbosduwh@sdu.edu.cn (B. Song), maixianmin@foxmail.com (X. Mai), mayongfn@gmail.com (Y. Ma), zguo10@utk.edu (Z. Guo).

https://doi.org/10.1016/j.compositesb.2018.09.081
Received 9 September 2018; Received in revised form 17 September 2018; Accepted 24 September 2018
Available online 25 September 2018
1359-8368/

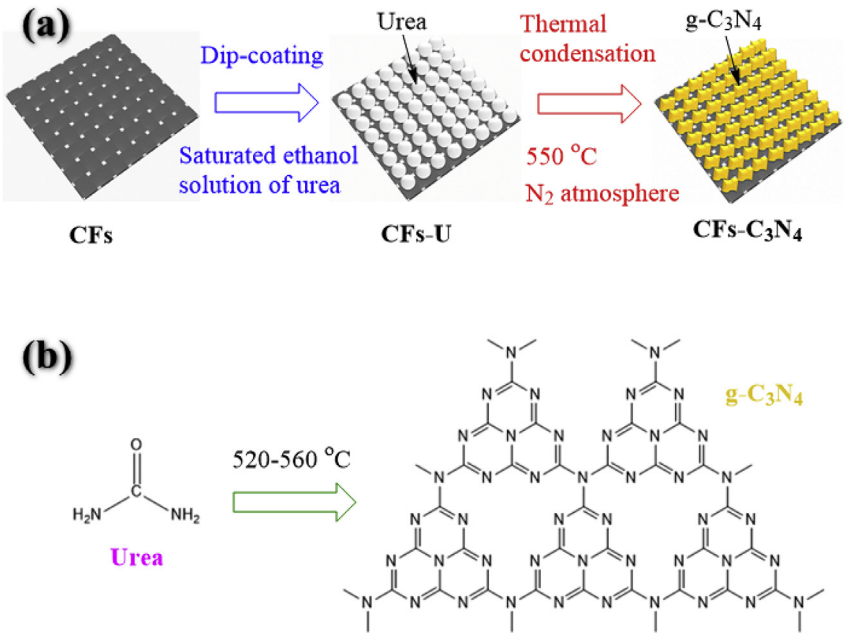

Fig. 1. Schematic illustration of (a) in-situ synthesis of g-C_3N_4 on CFs surface; (b) synthesis process of g-C_3N_4 by thermal polymerization of urea.

approaches, in-situ synthesis can regulate the interphase structure more effectively, ameliorate the interfacial compatibility and strengthen the interfacial adhesion.

The properties of the interphase containing nanomaterials are dependent to a great extent on the inherent properties of the nanomaterials [38–40]. In previous research reports, carbon nanotubes (CNTs) [41–43], graphene/graphene oxide (GO) [44–47], ZnO nanowires [48,49] and TiO_2 nanorods [50,51] etc. were successfully applied in the construction of interphase of composites. For example, Sharma and his co-worker [52] synthesized CNTs and nanofibers on CF substrate using thermal chemical vapor deposition (CVD) process. The composites made of CNTs coated CF showed 69% higher tensile strength as compared to the composites made of original CFs. Wang et al. [53] found that the grafting force between CNTs and CF created by CVD was so strong (up to 5 μN) that the interfacial shear strength of CF composites was increased by 30%. Zheng et al. [54] used ZnO nanowires to construct the interphase of CF composites through a facial hydrothermal method. The interfacial shear strength of CF composites was increased by 64% after the in-situ growth of ZnO nanowires on the CF surface. Due to the rigid ZnO nanowires that can more effectively improve the toughness of CF composites compared to those flexible fillers (like CNTs) with easy collapse during epoxy infusion, both mode I and mode II interlaminar toughness of CF composites laminates were increased by 63% and 22%, respectively. Meanwhile, the introduction of nanomaterials can significantly change the physical and chemical properties of interphase. Harpreet et al. [8] confirmed that the relative interphase size and interfacial area were increased by approximately 3 times in the presence of CNTs. The gradual variation in modulus from epoxy to CF through the interphase region containing CNTs effectively suppressed the unwanted stress concentrations around the CF due to the existence of sharp interface, thus markedly enhanced the stiffness, IFSS and load bearing capacity of CF composites. Although the research on interfacially reinforced CF composites by constructing interphase containing nanomaterials has made many significant progress, enormous potential of interphase containing nanomaterials has not been fully exploited. Some new materials should be explored in the construction of interphase of CF composites.

In this study, graphitic carbon nitride (g-C_3N_4) as a conjugated polymer with graphite-like structure was used to construct the interphase of CF composites via an in-situ synthesis process. The interphase created by g-C_3N_4 markedly improved the compatibility between CF and matrix, and endowed CF composites with superior interfacial properties than that of other CF composites. Meanwhile, the surface morphology and fracture appearance of CF and its composites were observed by scanning electron microscope (SEM). Surface chemical elements, functional group and phase structure of CF and g-C_3N_4 were investigated by X-ray photoelectron spectroscopy (XPS), Fourier Transform Infrared Spectroscopy (FTIR) and X-ray diffraction (XRD), respectively. Wettability studies were carried out on a dynamic contact angle analysis (DCAT). The interfacial compatibility between CF and epoxy was evaluated by interfacial shear strength (IFSS), interlaminar shear strength (ILSS), impact toughness and hydrothermal aging resistance. Moreover, the practical application of CF composites was also explored by dynamic thermomechanical analysis (DMA).

2. Materials and experiments

2.1. Materials

The plain weave carbon fiber fabric (T300 3 K, diameter: 7 μm, surface density: 200 g/cm^2) used in this study was purchased from Guangwei Co. Ltd (China). The carbon fiber fabric was thermally treated at 450 °C for 1 h in N_2 environment to remove the sizing (the obtained samples were denoted as CFs). Epoxy resin (HT-723A-1) and curing agent (HT-723B-1) were supplied from Wells Advanced Materials (shanghai) Co., Ltd (China). Urea, absolute ethanol and acetone were purchased from Aladdin (China). All chemicals, reagents and solvents were of analytical grade and used as received without further purification.

2.2. Surface treatment of CFs fabric

The in-situ synthesis of g-C_3N_4 on carbon fiber fabric was realized through a combination of dip-coating and thermal condensation method. The schematic formation of g-C_3N_4 on CFs surface is shown in Fig. 1(a). A typical synthesis process is as follows. First, the CFs were immersed in saturated ethanol solution of urea for 40 min and dried at 80 °C for 5 h (the CFs coated with urea were called as CFs-U). Then the CFs-U were embedded into powders of urea and calcined at 550 °C for 4 h under a N_2 atmosphere (the synthesis process of g-C_3N_4 was

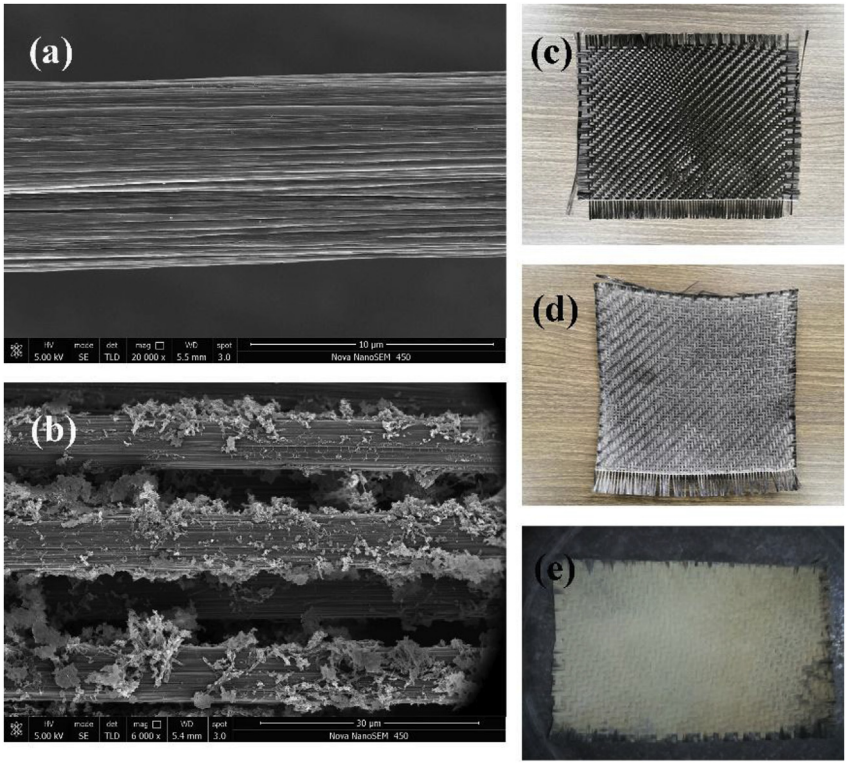

Fig. 2. Surface morphology of carbon fiber fabric: (a)/(c) CFs; (b)/(d) CFs-C_3N_4; (c) CFs-U.

illustrated in Fig. 1(b)). This as-prepared CFs fabric was ultrasonically washed in absolute ethanol to remove the loosened g-C_3N_4 on the CF surface, followed by drying at 80 °C for 4 h in a vacuum drying oven (the obtained samples were named as CFs-C_3N_4). Moreover, pure g-C_3N_4 was also synthesized under the same conditions.

2.3. Preparation of CF composite laminates

CF composite laminates comprising of eight plies of plain weave CF fabric (with/without g-C_3N_4) were fabricated via a vacuum bag-pressure moulding. The CF composite laminates were pre-formed by vacuum bag moulding and left to cure at 50 °C for 2 h. Then the laminates were post-cured via pressure moulding at 90 °C for 3 h (moulding pressure for 10 MPa). The cured laminates were respectively machined into ASTM D3039 tensile coupons (175 mm length × 25 mm width × 2 mm thick), ASTM D7264 flexural coupons (155 mm length × 13 mm width × 4 mm thick) and ASTM D2344 shear coupons (24 mm length × 8 mm width × 4 mm thick) using a diamond saw.

2.4. Characterizations

The surface morphologies of CF fabric and fracture surface features were detected by SEM (HITACHI, FE-SEM SU8000). The chemical binding states of CF fabric were characterized by X-ray photoelectron spectroscopy (XPS, K-Alpha Compact, Thermo Scientific). The surface functional groups of CF fabric were investigated by Fourier transform infrared spectroscopy (FTIR, VERTEX70, Bruker). The phase structures of CF and g-C_3N_4 were characterized using X-ray diffraction (XRD, Rigaku D/max-rB). Thermogravimetry (TG) analysis of CFs was carried out on a DSC/DTA TG simultaneous thermal analyzer (STA 449 F5 Jupiter, NETZSCH) from 30 to 800 °C at a heating rate of 10 °C/min.

The wettability between CF and epoxy was evaluated by dynamic contact angle test using a dynamic contact angle meter and tensiometer (DCAT21, DataPhysics Instruments). Deionized water (γ_s^d = 21.8 mN/m, γ_s = 72.8 mN/m) and diiodomethane (γ_s^d = 50.8 mN/m, γ_s = 50.8 mN/m) were used as test liquids for the determination of surface energies (γ_s), dispersive component (γ_s^d) and polar component (γ_s^p) of CFs.

The mechanical properties were evaluated using a universal testing machine (E45.305, MTS). The tensile strength of CF monofilament was tested in accordance with ASTM D3379-75 (no fewer than 60 samples were evaluated), and the obtained data were processed using Wellbull statistical method. The interfacial shear strength (IFSS) of CF composites was measured by micro-droplet experiment, which was performed on an evaluation device for interfacial adhesion of composites (HM410, MODEL) at the crosshead speed of 0.08 mm/s. The IFSS was calculated by Eq. (1), where d, L and F represent diameter of CF monofilament, embedded length of resin droplet and maximum pull-out force, respectively.

$$IFSS = \frac{F}{\pi dL} \tag{1}$$

The interlaminar shear strength (ILSS) of CF composite laminates was evaluated by a three-point short beam bending according to ASTM D2344 standard at a crosshead speed of 2 mm/min. Then ILSS was calculated according to Eq. (2), where P_b, h and d represent the breaking load, width and thickness of specimen, respectively. The tensile test was implemented on the basis of ASTM D3039 at a constant crosshead rate of 2 mm/min. The flexural properties were obtained by three-point bending according to ASTM D7264 standard at a constant rate of crosshead movement of 1.0 mm/min. Each used data for mechanical properties of CF composite laminates was an averaged value of 6 specimens.

$$ILSS = \frac{3P_b}{4bh} \tag{2}$$

The impact toughness was assessed using a pendulum impact test system (9250HV, Instron). The span of tested samples was set to 40 mm, the weight and velocity of pendulum were selected as 3 kg and 2 m/s, respectively. Each specimen was repeatedly tested at least six times. Dynamic mechanical experiment was implemented on a dynamic

mechanical thermal analyzer (Q800, TA) operating in the three-point bending mode at a frequency of 1.0 Hz. The dimensions of specimen was 60 mm × 10 mm × 2 mm. The temperature range of experiment was limited to 30–180 °C with a heating rate of 3 °C/min. The hydrothermal aging resistance of CF composite laminates was studied by tracing the change of ILSS after laminates immersed in the boiling water for 48 h. At least 5 samples were tested for the evaluation of hydrothermal aging resistance.

3. Results and discussion

3.1. Surface morphology and crystal phase of CF fabric

The surface morphology of carbon fiber fabric was illustrated in Fig. 2. The surface of untreated CFs was smooth and neat, and some grooves along the direction of fiber axis were uniformly distributed throughout the carbon fiber surface. After surface treatment, some marked changes of surface morphology can be found on the CFs-C_3N_4 surface. Some micron-sized g-C_3N_4 particles were uniformly distributed on the surface of CFs-C_3N_4. Moreover, the appearance characteristics of carbon fiber fabric was also obtained by electronic photos (as shown in Fig. 2 (c) ~ (d)). Originally, the surface of CFs was neat and bright. The surface of CFs-U was then coated by a homogeneous layer of white urea after impregnation treatment. Lastly, the urea layer on carbon fiber fabric was changed into light-yellow g-C_3N_4 through a thermal polymerization. The existence of g-C_3N_4 particles greatly increased the surface roughness of carbon fibers and interfacial contact area in carbon fiber composite laminates.

Besides, the structure and composition of carbon fiber fabric were confirmed by XRD. As shown in Fig. 3(a), the observed only broad characteristic diffraction peak at around 23.0° is assigned to the (002) plane of graphitic structure of CFs [55]. Pure g-C_3N_4 has two characteristic diffraction peaks at 13.1° and 27.4°, respectively. The diffraction peak at 13.1° is attributed to the (100) plane resulting from the in-plane ordering of tri-*s*-triazine units with a distance of 0.670 nm, and the diffraction peak center at 27.4° is normally associated with the (002) plane due to the interlayer stacking reflection of conjugated aromatic structures with an interlayer space of 0.323 nm [56]. In comparison with CFs and pure g-C_3N_4, CFs-C_3N_4 exhibits the same diffraction peaks with pure g-C_3N_4 due to a large amount of g-C_3N_4 existing on the CFs-C_3N_4 surface.

3.2. Surface elemental composition of carbon fiber fabric

FTIR analysis in Fig. 3(b) reveals the surface functional groups of carbon fiber fabric and g-C_3N_4. No any significant characteristic absorption peak can be found on the FTIR curve of CFs, which means that the CF surface is inert. After impregnation treatment, the characteristic absorption peaks of urea appeared on the FTIR spectra of CFs-U. The characteristic absorption peaks centered at 1160 and 1450 cm^{-1} corresponded to the vibration mode and stretching mode of C—N bond, respectively [57]. The absorption peaks located in 1680–1630 cm^{-1} were attributed to the stretching vibration of C═O bond. The characteristic absorption peaks in the range of 900–650 and 3600–3100 cm^{-1} reflect the in-plane bending vibration and stretching vibration of N—H bond, respectively [57]. For the FTIR spectra of pure g-C_3N_4, the characteristic absorption peaks at around 1700–1200 cm^{-1} represent the stretching vibration of conjugated CN rings, and the

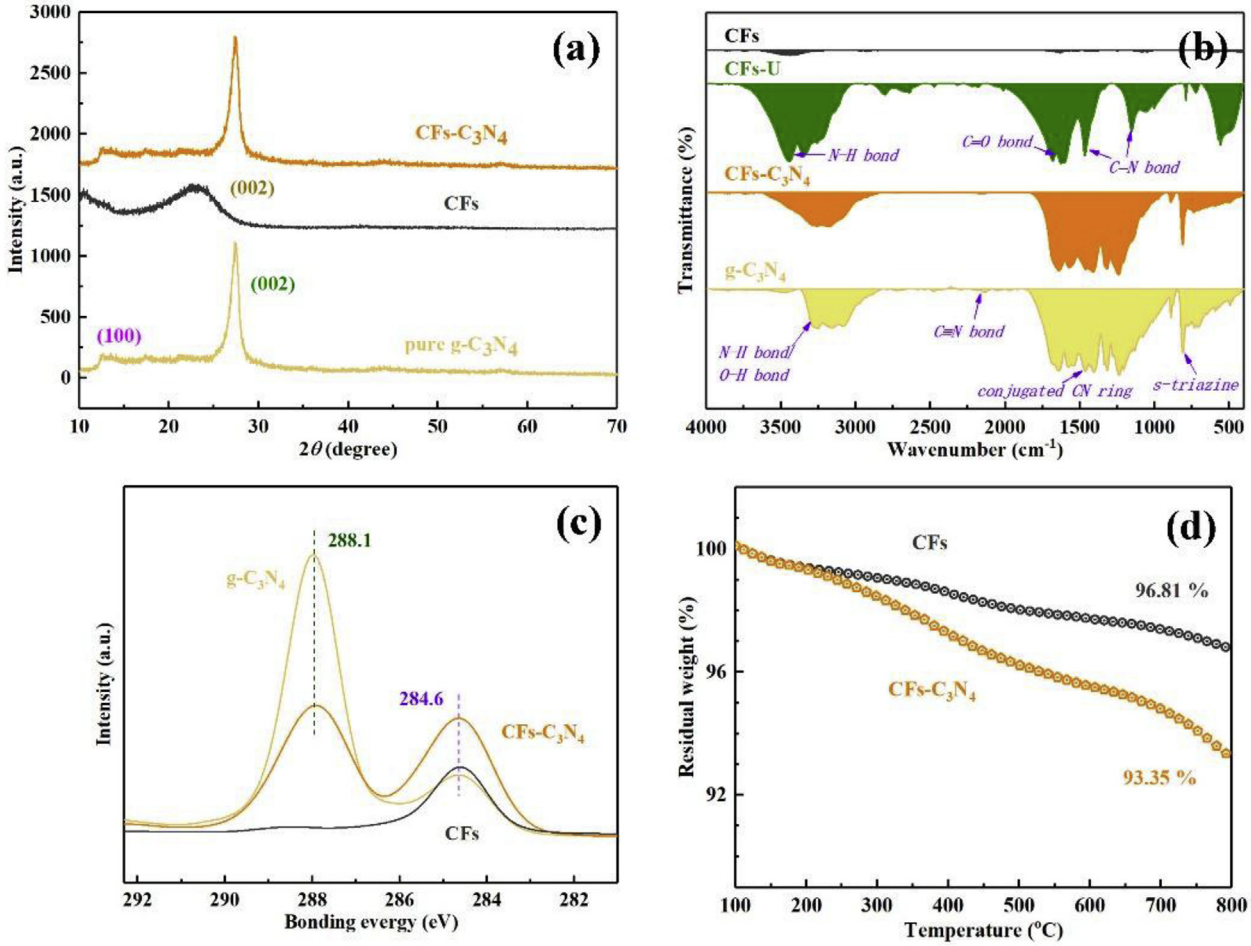

Fig. 3. Spectra of carbon fiber fabric and g-C_3N_4: (a) XRD; (b) FTIR; (c) XPS C1s; (d) TGA.

Table 1
Surface element composition of carbon fiber fabric and g-C_3N_4.

Sample	Element content (%)				
	C	O	N	O/C	N/C
CFs	88.59	10.23	1.18	11.55	1.33
g-C_3N_4	44.18	7.19	48.63	16.27	110.07
CFs-C_3N_4	50.68	5.79	43.53	11.42	85.89

absorption peaks centered at 806 and 2178 cm^{-1} were assigned to the breathing mode of s-triazine and C≡N triple bonds, respectively [58]. The characteristic absorption peaks in the range of 3500–3000 cm^{-1} were attributed to the stretching mode of O—H bond and the vibration mode of N—H bond [59]. Interestingly, the spectrum of CFs-C_3N_4 displays a similar absorption peak in the wavenumber range of 4000–400 cm^{-1} due to the formation of g-C_3N_4 on the carbon fiber surface. The increased surface functional groups on CFs-C_3N_4 surface can effectively improve the interfacial compatibility and strengthen the interfacial bonding between matrix and reinforcement.

In addition, the surface element composition of carbon fiber fabric was investigated by XPS. The detailed information on surface element composition of samples was summarized in Table 1. The surfaces of all samples are composed of carbon, oxygen and nitrogen element. Carbon is the main element on CF surface (88.59%), and the content of carbon and nitrogen on g-C_3N_4 surface is almost equal (44.18 and 48.63%, respectively). The formation of g-C_3N_4 results in a vast increase in the nitrogen content on the surface of CF fabric (increased by 35.89 times). Moreover, the XPS C1s spectra were also supplied for further understanding the chemical element state on CF surface. As shown in Fig. 3(c), the characteristic peak at about 284.6 eV for CFs sample reflects the sp^2 hybridized C atom in the C—C group [52]. Meanwhile, the XPS C1s spectra of g-C_3N_4 reveal two different characteristic peaks located at 284.6 and 288.1 eV, respectively. The characteristic peak centered at 288.1 eV is attributed to the sp^2-bonded C in N═C $(—N)_2$ group [60]. More significantly, the characteristic peak of sp^2-bond C in N═C $(—N)_2$ group appeared in the C1s spectra of CFs-C_3N_4 after the formation of g-C_3N_4 on CF fabric surface. Moreover, the existence of g-C_3N_4 was also proved by TGA test (Fig. 3(d)). Owing to the thermal degradation of surface materials in the temperature range of 50–800 °C, a weight loss of 3.19% was observed in the TGA curve of CFs. The TGA analysis of CFs-C_3N_4 embodies a higher weight loss of 6.65% due to the decomposition of g-C_3N_4. Therefore, a conclusion can be drawn from the above XPS and TGA analysis that g-C_3N_4 was successfully synthesized on the CF fabric surface.

3.3. Interfacial properties

The interfacial compatibility (or wettability) between reinforcement and matrix is generally affected by the surface energy of reinforcement. High surface energy equals to a better interfacial compatibility and stronger interfacial adhesion. Here, the surface energy of carbon fiber samples was measured by a Cahn dynamic angle analysis system. Table 2 provides a summary and comparison of contact angle (θ), surface energy (γ) and its sub-component (polar component: γ^p and dispersion component: γ^d). The de-sizing treatment of CFs causes a certain degree of reduction of surface energy from 41.90 to 35.45 mJ/m. Surprisingly, CFs-C_3N_4 exhibits a smaller contact angles and higher surface energy compared to that of CFs. The in-situ synthesis of g-C_3N_4 leads to the contact angle of CFs with deionized water (polar solvent) decreasing from 77.25° to 48.81°, the contact angle of CFs with diiodomethane (non-polar solvent) decreased from 61.47° to 36.13°. This change directly causes the surface energy of CFs-C_3N_4 rise from 35.45 to 59.49 mJ/m with an increase rate of 67.81%. The growth of γ^p (from 7.72 to 17.99 mJ/m) and γ^d (from 27.73 to 41.50 mJ/m) was attributed to the substantially increased surface roughness and functional groups created by g-C_3N_4. It is totally expected that the hierarchical structure of CFs-C_3N_4 with a high surface energy can more effectively ameliorate the interfacial compatibility between CFs and epoxy resin, thus significantly improves the interfacial properties of composites.

Table 2
Contact angle, surface energy and roughness of carbon fibers.

Sample	Contact angle (°)		Surface energy (mJ/m)		
	Deionized water	Diiodomethane	γ^d	γ^p	γ
As-received CFs	67.35	58.14	29.65	12.25	41.90
CFs	77.25	61.47	27.73	7.72	35.45
CFs-C_3N_4	48.81	36.13	41.50	17.99	59.49

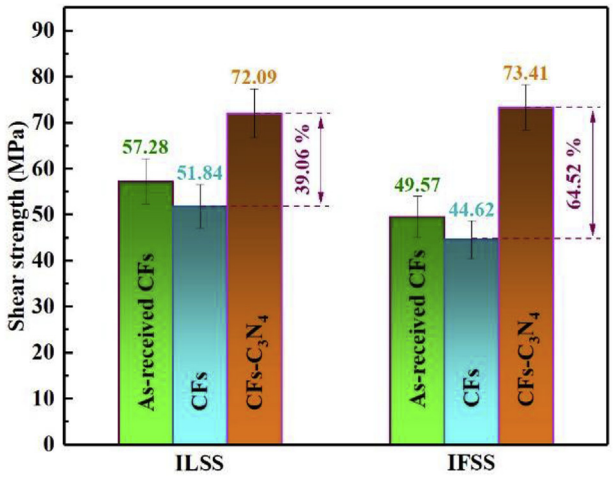

Fig. 4. IFSS and ILSS of carbon fiber and its composites laminates.

The good interfacial properties can endow composites with excellent mechanical properties. Here, ILSS as an important index of mechanical properties of CF composite laminates was assessed by three-point bending test. As illustrated in Fig. 4, compared with as-received CFs, the ILSS of CFs decreases in a certain extent (from 57.28 to 51.84 MPa) after de-sizing treatment. The introduction of g-C_3N_4 led to the ILSS of composite laminates made of CFs-C_3N_4 increase to 72.09 MPa with a rise rate of 39.06%. Besides, the IFSS as the frequent reference standard for interfacial adhesion between CFs and epoxy resin was also studied by micro-droplet debonding experiment. The IFSS exhibits the similar change trend with that of ILSS. The IFSS of CF composite laminates decreases firstly from 49.57 to 44.62 MPa due to de-sizing treatment, then increases to 73.41 MPa with a growth rate of 64.52% after the in-situ treatment. The significantly improved interfacial properties of composite laminates can be attributed to the massive increased mechanical interlocking and chemical bonding in the interphase formed during the surface modification [61]. The introduced g-C_3N_4 creates a better interfacial compatibility, bigger contact area and stronger mechanical interlocking for the interfacial bonding. Moreover, the open-ring reaction between amino groups on the g-C_3N_4 surface and epoxy groups of matrix provides a stronger chemical bonding for interfacial adhesion of composites.

3.4. Mechanical properties

The mechanical properties of CFs and its composite laminates were investigated using tensile and bending test. As shown in Fig. 5, the tensile strength (TS) of single carbon fiber for as-received CFs, CFs and CFs-C_3N_4 is 3.49, 3.47 and 3.56 GPa, respectively. The treatment process has a negligible impact on the mechanical properties of CFs. Besides, a comparison of mechanical properties for carbon fiber composite laminates was supplied in Fig. 5(b). The introduction of g-C_3N_4 on

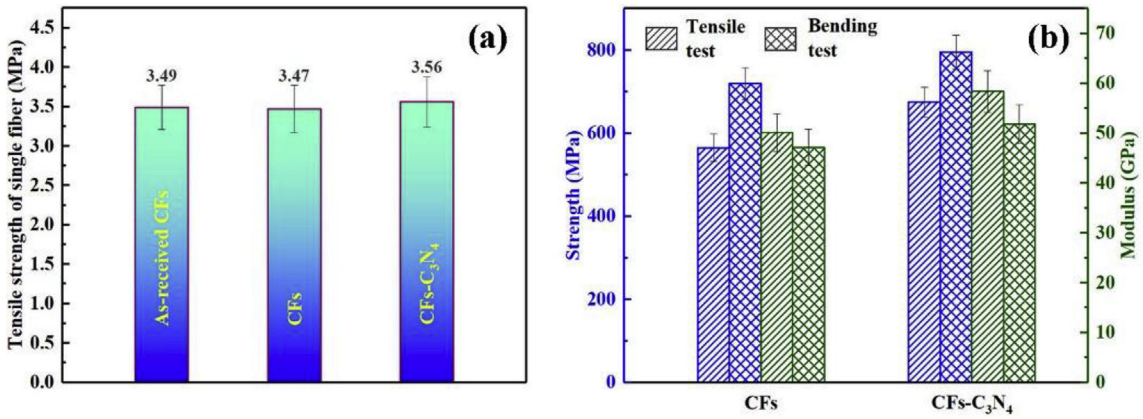

Fig. 5. Tensile test and bending test for carbon fibers fabric composite laminates.

carbon fiber fabric surface significantly enhanced the mechanical properties of carbon fiber composite laminates. The TS and tensile modulus of CF composite laminates are increased from 564.91 MPa to 675.31 MPa (increased by 19.54%) and from 50.12 GPa to 58.37 GPa (increased by 16.46%), respectively. Meanwhile, the bending strength and bending modulus have also been improved from 719.51 to 795.13 MPa (rise by 10.51%) and from 47.14 to 51.83 GPa (rise by 9.95%). The significantly enhanced mechanical properties of carbon fiber composite laminates can be attributed to the synergistic effects of increased wettability, mechanical interlocking and chemical bonding between CFs and epoxy resin result from the introduction of g-C_3N_4 [62].

Here, impact properties as an important index of mechanical properties of carbon fiber composite laminates were also explored. As illustrated in Fig. 6, the initial, propagative and total absorbed energy of CFs composite laminate was 0.21, 0.93 and 1.14 J, respectively. The impact properties of CFs-C_3N_4 composite laminates were greatly enhanced duo to the in-situ synthesis of g-C_3N_4. The initial, propagative and total absorbed energy was increased to 0.54, 1.24 and 1.78 J, respectively. Generally, the interphase of carbon fiber composite laminates as a protective layer can absorb the fracture energy through triggering cracks and sub-cracks, thus holds back the direct contact between crack tips and CFs [63]. Obviously, the complex structure of interphase containing g-C_3N_4 can cause more cracks and sub-cracks, dissipate more destructive energy, thus effectively improves the impact failure resistance. Meanwhile, the failure surface morphology of carbon fiber composite laminates was further explored for impact properties

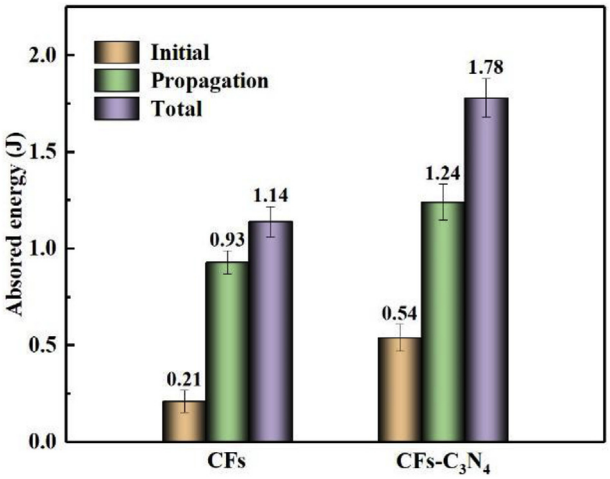

Fig. 6. Impact properties of carbon fibers composite laminates reinforced with CFs and CFs-C_3N_4, respectively.

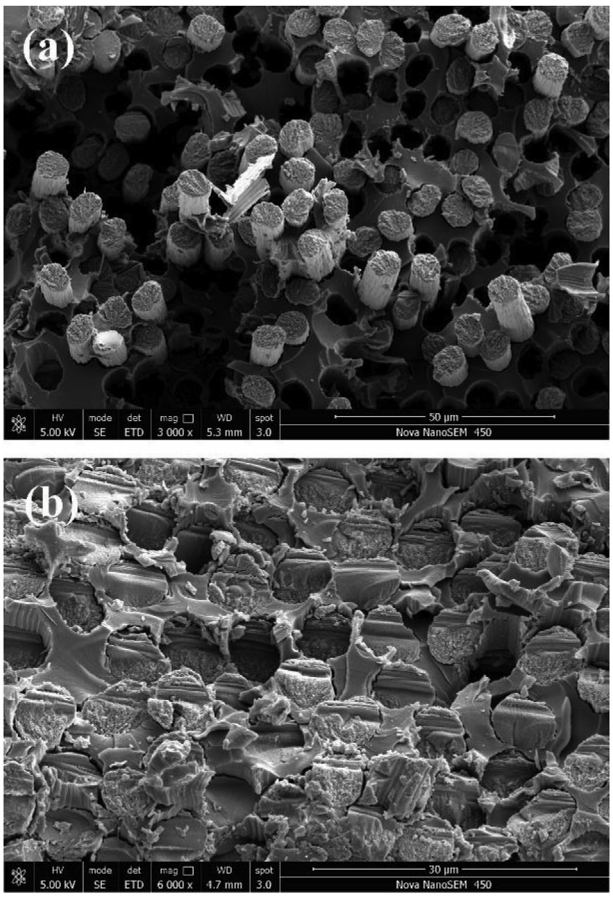

Fig. 7. Failure surface morphology for carbon fibers composite laminates: (a) CFs and (b) CFs-C_3N_4.

(Fig. 7). Interfacial de-bonding, cracks and pull-out of fiber are found on the fracture surface of CF composite laminates due to poor interfacial adhesion. The flat fracture morphology of CFs-C_3N_4 indicates a stronger interfacial adhesion supplied by better wettability, increased mechanical interlocking and enhanced chemical bonding exists in the interphase of composite laminates.

Base on the above analysis, an impact test model was depicted in Fig. 8 for revealing the mechanism of interphase in the composite laminates. For CF composite laminates, inferior interfacial adhesion created by simple structure of the thin interphase easily triggers a low effective load transfer between reinforcement and matrix, and a faster propagation of cracks along the interfacial area under a low applied

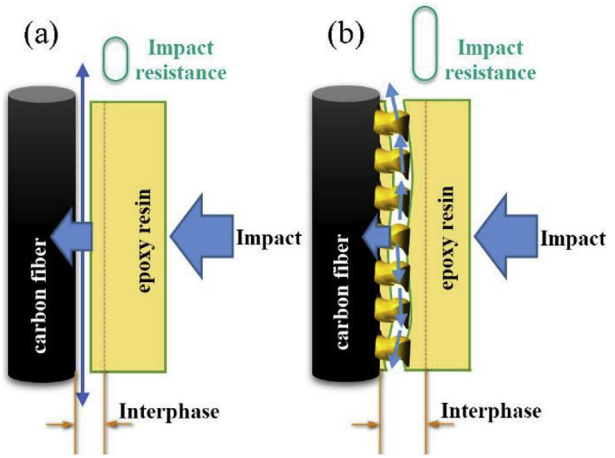

Fig. 8. Schematic impact test of carbon fibers composite laminates: (a) CFs and (b) CFs-C_3N_4.

load. In the case of CFs-C_3N_4 composite laminates, the powerful and complicated structure of the thick interphase provides stronger interfacial chemical bonding and mechanical interlocking force, thus effectively ameliorate the interfacial load transfer, promptly release the stress concentration and sharply dissipate the destructive energy [64]. Moreover, the complicated cracks propagation and improved deformation ability of matrix can promote the formation of micro-cracks and change of failure mode [65]. This complex propagation process of cracks can markedly enhance the impact properties through consuming more energy.

Furthermore, the dynamic mechanical properties were also investigated. Fig. 9 indicates the variation of storage modulus (E') and loss factor (tan δ) with temperature for carbon fiber composite laminates. Clearly, CFs-C_3N_4 composite laminates have a higher E' than that of CFs composite laminates. The introduction of g-C_3N_4 causes E' increase from 37.17 to 43.83 GPa below glass transition temperature (T_g) and from 7.65 to 16.40 GPa above T_g, which embodies a superior stability of stiffness at near T_g. This increased E' was ascribed to the enlarged interphase region and reduced mobility of polymer chains in the interphase [66]. Hence, the complex interphase constructed by g-C_3N_4 can act as an auxiliary reinforcement for mechanical stiffening of carbon fiber composite laminates. Interestingly, similar phenomena and conclusions were obtained in the CNT/CF composite system [67]. Meanwhile, the T_g of carbon fiber composite laminates was raised from 109.71 to 121.34 °C after the surface treatment. The enhancement of T_g can be attributed to the strengthened restricted-mobility of polymer chains in the interphase [68]. The high specific surface area and abundant surface functional groups of g-C_3N_4 significantly enhance the wettability and interaction between CFs and epoxy resin and increase the crosslinking degree in the interphase. Furthermore, the g-C_3N_4 can also restrain the viscous flow of polymer chains, thereby realize the energy loss minimization of viscous deformation.

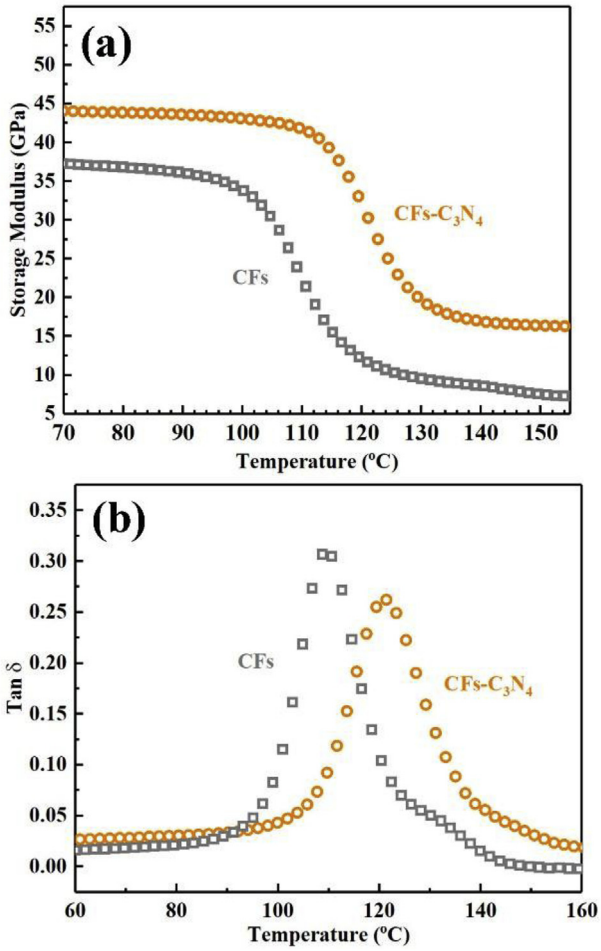

Fig. 9. Dynamic mechanical analysis of carbon fibers composite laminates: (a) storage modulus and (b) Tan δ.

3.5. Hydrothermal aging resistance

The performance and service life of CF composite laminates are often affected by the surrounding environment. For example, high humidity environments can hydrolyze and damage the interphase structure of CF composites, thus degrade the whole performance and life of composites. Here, hydrothermal aging resistance as an important embodiment of performance stability of CF composite laminates was evaluated. As illustrated in Fig. 10, a serious degradation in ILSS occurred after hydrothermal aging treatment. The IFSS of CFs and CFs-C_3N_4 was reduced by 31.29% (from 51.84 to 35.62) and 18.89% (from 72.09 to 58.47), respectively. The interfacial adhesion of CFs composite

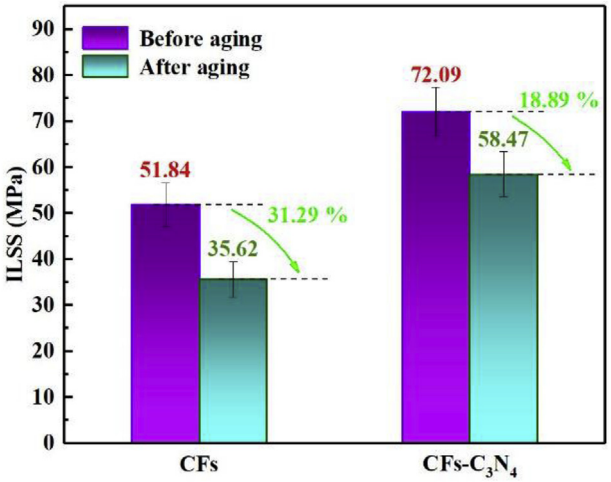

Fig. 10. Change of ILSS before and after hydrothermal aging for 48 h.

laminates is so poor that water molecules can easily penetrate into the interphase, thus severely destroy the interfacial structure and substantially degrade the interfacial properties [69,70]. The markedly improved hydrothermal aging resistance of CFs-C_3N_4 composite laminates was ascribed to the strong and powerful interfacial adhesion created by the increased mechanical interlocking and chemical bonding between CFs and epoxy resin [71–74]. In addition, the damage of C—N

bond created by opening-ring reaction between amino groups on g-C_3N_4 surface and epoxy groups of matrix can consume more destructive energy, thus enhances the structural stability of interphase [75–99].

4. Conclusions

Here, g-C_3N_4 was used to structure the interphase of carbon fiber composite laminates for interfacial strengthening via an in-situ synthesis. The existence of g-C_3N_4 greatly increased surface roughness, surface functional groups and surface free energy of carbon fibers, thus significantly enhance the interfacial properties of carbon fibers composite. Surface free energy was increased from 35.45 to 59.49 mJ/m. The ILSS and IFSS of carbon fiber composite laminates were enhanced from 51.84 to 72.09 MPa and 44.62–73.41 MPa, respectively. The significantly improved interfacial properties guarantee excellent mechanical properties of carbon fiber composite laminate. Tensile strength and bending strength of composite laminates were increased from 564.91 to 675.31 MPa and 719.51–795.13 MPa, respectively. Total absorbed energy of impact test was increased from 1.14 to 1.78 J. Furthermore, dynamic mechanical properties and hydrothermal aging resistance were also improved significantly. The T_g was increased from 109.71 to 121.34 °C. The E' of composite laminates was increased from 37.17 to 48.83 GPa below T_g and from 7.65 to 16.40 GPa above T_g, respectively. The hydrothermal aging test confirms that the ILSS of carbon fiber composite laminates was decreased from 31.29 to 18.89%. The markedly enhanced interfacial properties and mechanical properties of CFs-C_3N_4 composite laminates can be attributed to the increased mechanical interlocking, enhanced chemical bonding and ameliorated wettability due to the existence of g-C_3N_4 on carbon fibers surface. With the inherent lightweight as compared with metals and ceramics, the surface modification mentioned in this study not only can be used for the interfacial strengthening of composite laminates, but also can be applied in other fields, such as environmental governance, energy development and ultra-capacitor [78–82].

Declaration of interest

The authors declare no conflict of interest regarding the publication of this paper.

Acknowledgements

This work is financially supported by the National Natural Science Foundation of China (Grant Nos. 51603115) and Key Research and Development Program of Shandong Province (China, Grant Nos. 2017GGX20142).

References

[1] Agnihotri P, Basu S, Kar KK. Effect of carbon nanotube length and density on the properties of carbon nanotube-coated carbon fiber/polyester composites. Carbon 2011;49(9):3098–106.
[2] Cheng C, Fan R, Wang Z, Shao Q, Guo X, Xie P, et al. Tunable and weakly negative permittivity in carbon/silicon nitride composites with different carbonizing temperatures. Carbon 2017;125:103–12.
[3] Cheng XQ, Wang ZX, Jiang X, Li T, Lau CH, Guo Z, et al. Towards sustainable ultrafast molecular-separation membranes: from conventional polymers to emerging materials. Prog Mater Sci 2018;92:258–83.
[4] Jiang X, Li S, He S, Bai Y, Shao L. Interface manipulation of CO_2–philic composite membranes containing designed UiO-66 derivatives towards highly efficient CO_2 capture. J Mater Chem 2018;6:15064–73.
[5] Cui X, Zhu G, Pan Y, Shao Q, Zhao C, Dong M, et al. Polydimethylsiloxane-titania nanocomposite coating: fabrication and corrosion resistance. Polymer 2018;138:203–10.
[6] Du H, Zhao CX, Lin J, Guo J, Wang B, Hu Z, et al. Carbon nanomaterials in direct fiquid fuel cells. Chem Rec 2018;18(9):1365–72.
[7] Gong K, Guo S, Zhao Y, Hu Q, Liu H, Sun D, et al. Bacteria cell templated porous polyaniline facilitated detoxification and recovery of hexavalent chromium. J Mater Chem 2018;6(35):16824–32.
[8] Bedi HS, Tiwari M, Agnihotri PK. Quantitative determination of size and properties of interphases in carbon nanotube-based multiscale composites. Carbon 2018;132:181–90.
[9] Sun H, Yang X, Zhang Y, et al. Segregation-induced in situ hydrophilic modification of poly (vinylidene fluoride) ultrafiltration membranes via sticky poly (ethylene glycol) blending. J Membr Sci 2018;563:22–30.
[10] Gu H, Zhang H, Lin J, Shao Q, Young DP, Sun L, et al. Large negative giant magnetoresistance at room temperature and electrical transport in cobalt ferrite-polyaniline nanocomposites. Polymer 2018;143:324–30.
[11] Gu J, Li Y, Liang C, Tang Y, Tang L, Zhang Y, et al. Synchronously improved dielectric and mechanical properties of wave-transparent laminated composites combined with outstanding thermal stability by incorporating iysozyme/POSS functionalized PBO fibers. J Mater Chem C 2018;6:7652–60.
[12] Guan X, Zheng G, Dai K, Liu C, Yan X, Shen C, et al. Carbon nanotubes-ddsorbed Electrospun PA66 nanofiber bundles with improved conductivity and robust flexibility. ACS Appl Mater Interfaces 2016;8(22):14150–9.
[13] Yang X, Wang Z, Shao L. Construction of oil-unidirectional membrane for integrated oil collection with lossless transportation and oil-in-water emulsion purification. J Membr Sci 2018;549:67–74.
[14] Du X, Liu H-Y, Xu F, Zeng Y, Mai Y-W. Flame synthesis of carbon nanotubes onto carbon fiber woven fabric and improvement of interlaminar toughness of composite laminates. Compos Sci Technol 2014;101:159–66.
[15] Du X, Zhou H, Sun W, Liu H-Y, Zhou G, Zhou H, et al. Graphene/epoxy interleaves for delamination toughening and monitoring of crack damage in carbon fibre/epoxy composite laminates. Compos Sci Technol 2017;140:123–33.
[16] Guo J, Song H, Liu H, Luo C, Ren Y, Ding T, et al. Polypyrrole-interface-functionalized nano-magnetite epoxy nanocomposites as electromagnetic wave absorbers with enhanced flame retardancy. J Mater Chem C 2017;5(22):5334–44.
[17] Guo Y, Xu G, Yang X, Ruan K, Ma T, Zhang Q, et al. Significantly enhanced and precisely modeled thermal conductivity in polyimide nanocomposites with chemically modified graphene via in situ polymerization and electrospinning-hot press technology. J Mater Chem C 2018;6(12):3004–15.
[18] Xie P, Dang F, He B, Lin J, Fan R, et al. Bio-gel derived nickel/carbon nanocomposites with enhanced microwave absorption. J Mater Chem C 2018;6:8812–22.
[19] Fan W, Wang Y, Wang C, Chen J, Wang Q, Yuan Y, et al. High efficient preparation of carbon nanotube-grafted carbon fibers with the improved tensile strength. Appl Surf Sci 2016;364:539–51.
[20] Fredi G, Dorigato A, Fambri L, Pegoretti A. Multifunctional epoxy/carbon fiber laminates for thermal energy storage and release. Compos Sci Technol 2018;158:101–11.
[21] He Y, Yang S, Liu H, Shao Q, Chen Q, Lu C, et al. Reinforced carbon fiber laminates with oriented carbon nanotube epoxy nanocomposites: magnetic field assisted alignment and cryogenic temperature mechanical properties. J Colloid Interface Sci 2018;517:40–51.
[22] Hou Q, Ren J, Chen H, Yang P, Shao Q, Zhao M, et al. Synergistic hematite-fullerene electron-extracting layers for improved efficiency and stability in perovskite solar cells. ChemElectroChem 2018;5(5):726–31.
[23] Guo J, Zhang Q, Gao L, Zhong W, Sui G, Yang X. Significantly improved electrical and interlaminar mechanical properties of carbon fiber laminated composites by using special carbon nanotube pre-dispersion mixture. Compos Appl Sci Manuf 2017;95:294–303.
[24] Wang C, Mo B, He Z, et al. Hydroxide ions transportation in polynorbornene anion exchange membrane. Polymer 2018;138:363–8.
[25] Hu C, Li Z, Wang Y, Gao J, Dai K, Zheng G, et al. Comparative assessment of the strain-sensing behaviors of polylactic acid nanocomposites: reduced graphene oxide or carbon nanotubes. J Mater Chem C 2017;5(9):2318–28.
[26] Hu W, Liu T, Yin X, Liu H, Zhao X, Luo S, et al. Hematite electron-transporting layers for environmentally stable planar perovskite solar cells with enhanced energy conversion and lower hysteresis. J Mater Chem 2017;5(4):1434–41.
[27] Zhao J, Wu L, Zhan C, Shao Q, Guo Z, Zhang L. Overview of polymer nanocomposites: computer simulation understanding of physical properties. Polymer 2017;133:272–87.
[28] Felisberto M, Tzounis L, Sacco L, Stamm M, Candal R, Rubiolo GH, et al. Carbon nanotubes grown on carbon fiber yarns by a low temperature CVD method: a significant enhancement of the interfacial adhesion between carbon fiber/epoxy matrix hierarchical composites. Compos Comm 2017;3:33–7.
[29] Gong Q-J, Li H-J, Wang X, Fu Q-G, Wang Z-W, Li K-Z. In situ catalytic growth of carbon nanotubes on the surface of carbon cloth. Compos Sci Technol 2007;67(14):2986–9.
[30] Kang H, Cheng Z, Lai H, Ma H, Liu Y, Mai X, et al. Superlyophobic anti-corrosive and self-cleaning titania robust mesh membrane with enhanced oil/water separation. Separ Purif Technol 2018;201:193–204.
[31] Han W, Zhang H-P, Tavakoli J, Campbell J, Tang Y. Polydopamine as sizing on carbon fiber surfaces for enhancement of epoxy laminated composites. Compos Appl Sci Manuf 2018;107:626–32.
[32] Song B, Wang T, Sun H, Shao Q, Zhao J, Song K, et al. Two-step hydrothermally synthesized carbon nanodots/WO3 photocatalysts with enhanced photocatalytic performance. Dalton Trans 2017;46(45):15769–77.
[33] Li Y, Zhou B, Zheng G, Liu X, Li T, Yan C, et al. Continuously prepared highly conductive and stretchable SWNT/MWNT synergistically composited electrospun thermoplastic polyurethane yarns for wearable sensing. J Mater Chem C 2018;6(9):2258–69.
[34] Hung KH, Kuo WS, Ko TH, Tzeng SS, Yan CF. Processing and tensile characterization of composites composed of carbon nanotube-grown carbon fibers. Compos Appl Sci Manuf 2009;40(8):1299–304.
[35] Lin J, Chen X, Chen C, Hu J, Zhou C, Cai X, et al. Durably antibacterial and bacterially antiadhesive cotton fabrics coated by cationic fluorinated polymers. ACS

Appl Mater Interfaces 2018;10(7):6124–36.
[36] Liu H, Dong M, Huang W, Gao J, Dai K, Guo J, et al. Lightweight conductive graphene/thermoplastic polyurethane foams with ultrahigh compressibility for piezoresistive sensing. J Mater Chem C 2017;5(1):73–83.
[37] Luo F, Liu X, Shao C, Zhang J, Shen C, Guo Z. Micromechanical analysis of molecular orientation in high-temperature creep of polycarbonate. Mater Des 2018;144:25–31.
[38] Mirjalili V, Ramachandramoorthy R, Hubert P. Enhancement of fracture toughness of carbon fiber laminated composites using multi wall carbon nanotubes. Carbon 2014;79:413–23.
[39] Naghashpour A, Hoa SV. In situ monitoring of through-thickness strain in glass fiber/epoxy composite laminates using carbon nanotube sensors. Compos Sci Technol 2013;78:41–7.
[40] Naresh K, Shankar K, Rao BS, Velmurugan R. Effect of high strain rate on glass/carbon/hybrid fiber reinforced epoxy laminated composites. Compos B Eng 2016;100:125–35.
[41] Lachman N, Wiesel E, Guzman de Villoria R, Wardle BL, Wagner HD. Interfacial load transfer in carbon nanotube/ceramic microfiber hybrid polymer composites. Compos Sci Technol 2012;72(12):1416–22.
[42] Lisi N, Giorgi R, Re M, Dikonimos T, Giorgi L, Salernitano E, et al. Carbon nanowall growth on carbon paper by hot filament chemical vapour deposition and its microstructure. Carbon 2011;49(6):2134–40.
[43] Lomov SV, Gorbatikh L, Houlle M, Kotanjac Ž, Koissin V, Vallons K, et al. Compression resistance and hysteresis of carbon fibre tows with grown carbon nanotubes/nanofibres. Compos Sci Technol 2011;71(15):1746–53.
[44] Kandare E, Khatibi AA, Yoo S, Wang R, Ma J, Olivier P, et al. Improving the through-thickness thermal and electrical conductivity of carbon fibre/epoxy laminates by exploiting synergy between graphene and silver nano-inclusions. Compos Appl Sci Manuf 2015;69:72–82.
[45] Lubineau G, Rahaman A. A review of strategies for improving the degradation properties of laminated continuous-fiber/epoxy composites with carbon-based nanoreinforcements. Carbon 2012;50(7):2377–95.
[46] Mathur RB, Chatterjee S, Singh BP. Growth of carbon nanotubes on carbon fibre substrates to produce hybrid/phenolic composites with improved mechanical properties. Compos Sci Technol 2008;68(7–8):1608–15.
[47] Song B, Wang T, Sun H, Liu H, Mai X, Wang X, et al. Graphitic carbon nitride (g-C3N4) interfacially strengthened carbon fiber epoxy composites. Compos Sci Technol 2018;167:515–21.
[48] Kong K, Deka BK, Kim M, Oh A, Kim H, Park Y-B, et al. Interlaminar resistive heating behavior of woven carbon fiber composite laminates modified with ZnO nanorods. Compos Sci Technol 2014;100:83–91.
[49] Luo Q, Ma H, Hao F, Hou Q, Ren J, Wu L, et al. Carbon nanotube based inverted flexible perovskite solar cells with all-inorganic charge contacts. Adv Funct Mater 2017;27(42).
[50] Liu Y, Luo J, Helleu C, Behr M, Ba H, Romero T, et al. Hierarchical porous carbon fibers/carbon nanofibers monolith from electrospinning/CVD processes as a high effective surface area support platform. J Mater Chem 2017;5(5):2151–62.
[51] Su T, Shao Q, Qin Z, Guo Z, Wu Z. Role of interfaces in two-dimensional photocatalyst for water splitting. ACS Catal 2018;8(3):2253–76.
[52] Sharma SP, Lakkad SC. Effect of CNTs growth on carbon fibers on the tensile strength of CNTs grown carbon fiber-reinforced polymer matrix composites. Compos Appl Sci Manuf 2011;42(1):8–15.
[53] Wang C, Li Y, Tong L, Song Q, Li K, Li J, et al. The role of grafting force and surface wettability in interfacial enhancement of carbon nanotube/carbon fiber hierarchical composites. Carbon 2014;69:239–46.
[54] Zheng N, Huang Y, Sun W, Du X, Liu H-Y, Moody S, et al. In-situ pull-off of ZnO nanowire from carbon fiber and improvement of interlaminar toughness of hierarchical ZnO nanowire/carbon fiber hydrid composite laminates. Carbon 2016;110:69–78.
[55] Qian H, Bismarck A, Greenhalgh ES, Shaffer MSP. Synthesis and characterisation of carbon nanotubes grown on silica fibres by injection CVD. Carbon 2010;48(1):277–86.
[56] Qian H, Bismarck A, Greenhalgh ES, Shaffer MSP. Carbon nanotube grafted silica fibres: characterising the interface at the single fibre level. Compos Sci Technol 2010;70(2):393–9.
[57] Rahmanian S, Suraya AR, Shazed MA, Zahari R, Zainudin ES. Mechanical characterization of epoxy composite with multiscale reinforcements: carbon nanotubes and short carbon fibers. Mater Des 2014;60:34–40.
[58] Rahmanian S, Suraya AR, Zahari R, Zainudin ES. Synthesis of vertically aligned carbon nanotubes on carbon fiber. Appl Surf Sci 2013;271:424–8.
[59] Sager RJ, Klein PJ, Lagoudas DC, Zhang Q, Liu J, Dai L, et al. Effect of carbon nanotubes on the interfacial shear strength of T650 carbon fiber in an epoxy matrix. Compos Sci Technol 2009;69(7–8):898–904.
[60] Wang H, Moore JJ. Low temperature growth mechanisms of vertically aligned carbon nanofibers and nanotubes by radio frequency-plasma enhanced chemical vapor deposition. Carbon 2012;50(3):1235–42.
[61] Wang P, Yang J, Liu W, Tang X-Z, Zhao K, Lu X, et al. Tunable crack propagation behavior in carbon fiber reinforced plastic laminates with polydopamine and graphene oxide treated fibers. Mater Des 2017;113:68–75.
[62] Wang Y, Raman Pillai SK, Che J, Chan-Park MB. High interlaminar shear strength enhancement of carbon fiber/epoxy composite through fiber- and matrix-anchored carbon nanotube networks. ACS Appl Mater Interfaces 2017;9(10):8960–6.
[63] Wong DWY, Lin L, McGrail PT, Peijs T, Hogg PJ. Improved fracture toughness of carbon fibre/epoxy composite laminates using dissolvable thermoplastic fibres. Compos Appl Sci Manuf 2010;41(6):759–67.
[64] Xiong C, Li T, Zhao T, Dang A, Li H, Ji X, et al. Reduced graphene oxide-carbon nanotube grown on carbon fiber as binder-free electrode for flexible high-performance fiber supercapacitors. Compos B Eng 2017;116:7–15.
[65] Xu F, Du X-S, Liu H-Y, Guo W-G, Mai Y-W. Temperature effect on nano-rubber toughening in epoxy and epoxy/carbon fiber laminated composites. Compos B Eng 2016;95:423–32.
[66] Yamamoto N, John Hart A, Garcia EJ, Wicks SS, Duong HM, Slocum AH, et al. High-yield growth and morphology control of aligned carbon nanotubes on ceramic fibers for multifunctional enhancement of structural composites. Carbon 2009;47(3):551–60.
[67] Zeng Y, Liu H-Y, Mai Y-W, Du X-S. Improving interlaminar fracture toughness of carbon fibre/epoxy laminates by incorporation of nano-particles. Compos B Eng 2012;43(1):90.
[68] Zhang Q, Liu J, Sager R, Dai L, Baur J. Hierarchical composites of carbon nanotubes on carbon fiber: influence of growth condition on fiber tensile properties. Compos Sci Technol 2009;69(5):594–601.
[69] Zhong XH, Li YL, Feng JM, Kang YR, Han SS. Fabrication of a multifunctional carbon nanotube "cotton" yarn by the direct chemical vapor deposition spinning process. Nanoscale 2012;4(18):5614–8.
[70] Sun K, Fan R, Zhang X, Zhang Z, Shi Z, Wang N, et al. An overview of metamaterials and their achievements in wireless power transfer. J Mater Chem C 2018;6(12):2925–43.
[71] Zhou G, Yao H, Zhou Y, Wang W, Peng M. Self-assembled complexes of graphene oxide and oxidized vapor-grown carbon fibers for simultaneously enhancing the strength and toughness of epoxy and multi-scale carbon fiber/epoxy composites. Carbon 2018;137:6–18.
[72] Wang C, Murugadoss V, Kong J, He Z, Mai X, Shao Q, et al. Overview of carbon nanostructures and nanocomposites for electromagnetic wave shielding. Carbon 2018;140:696–733.
[73] Wang X, Liu X, Yuan H, Liu H, Liu C, Li T, et al. Non-covalently functionalized graphene strengthened poly(vinyl alcohol). Mater Des 2018;139:372–9.
[74] Wang Z, Wei R, Gu J, Liu H, Liu C, Luo C, et al. Ultralight, highly compressible and fire-retardant graphene aerogel with self-adjustable electromagnetic wave absorption. Carbon 2018;139:1126–35.
[75] Zhou H, Du X, Liu H-Y, Zhou H, Zhang Y, Mai Y-W. Delamination toughening of carbon fiber/epoxy laminates by hierarchical carbon nanotube-short carbon fiber interleaves. Compos Sci Technol 2017;140:46–53.
[76] Zhao M, Meng L, Ma L, Ma L, Yang X, Huang Y, et al. Layer-by-layer grafting CNTs onto carbon fibers surface for enhancing the interfacial properties of epoxy resin composites. Compos Sci Technol 2018;154:28–36.
[77] Zhou B, Li Y, Zheng G, Dai K, Liu C, Ma Y, et al. Continuously fabricated transparent conductive polycarbonate/carbon nanotube nanocomposite films for switchable thermochromic applications. J Mater Chem C 2018;6(31):8360–71.
[78] Pan Y, Schubert DW, Ryu JE, Wujick E, Liu C, Shen C, et al. Dynamic oscillatory rheological properties of polystyrene/poly(methyl methacrylate) blends and their composites in the presence of carbon black. Engineered Science 2018;1:86–94www.doi.org/10.30919/es.180402.
[79] Yang X, Liang C, Ma T, Guo Y, Kong J, Gu J, et al. A review on thermally conductive polymeric composites: classification, measurement, model and equations, mechanism and fabrication methods. Adv. Compos Hybrid Mater 2018;1(2):207–30.
[80] Zhao Z, Guan R, Zhang J, Zhao Z, Bai P. Effects of process parameters of semisolid stirring on microstructure of Mg-3Sn-1Mn-3SiC (wt%) strip processed by rheo-rolling. Acta Metall Sin (Engl Lett) 2017;30:66–72.
[81] Zhao Z, Bai P, Guan R, et al. Microstructural evolution and mechanical strengthening mechanism of Mg-3Sn-1Mn-1La alloy after heat treatments. Mater Sci Eng 2018;734:200–9.
[82] Zhang K, Li G-H, Feng L-M, Wang N, Guo J, Sun K, et al. Ultralow percolation threshold and enhanced electromagnetic interference shielding in poly(l-lactide)/multi-walled carbon nanotube nanocomposites with electrically conductive segregated networks. J Mater Chem C 2017;5(36):9359–69.
[83] Yang L, Wang X, Mai X, et al. Constructing efficient mixed-ion perovskite solar cells based on TiO_2 nanorod array. J Colloid Interface Sci 2018;534:459–68. https://doi.org/10.1016/j.jcis.2018.09.045. in press.
[84] Lu Y, Biswas M, Guo Z, Jeon J, Wujcik E. Recent developments in bio-monitoring via advanced polymer nanocomposite-based wearable strain sensors. Biosens Bioelectron 2018. https://doi.org/10.1016/j.bios.2018.08.037. in press.
[85] Yang Z, Hao X, Chen S, et al. Long-term antibacterial stable reduced graphene oxide nanocomposites loaded with cuprous oxide nanoparticles. J Colloid Interface Sci 2018;533:13–23.
[86] Hu Z, Zhang D, Lu F, et al. Multistimuli-responsive intrinsic self-healing epoxy resin constructed by host – guest interactions. Macromolecules 2018;51:5294–303.
[87] Li Z, Wang B, Qin X, et al. Superhydrophobic/superoleophilic polycarbonate/carbon nanotubes porous monolith for selective oil adsorption from water. ACS Sustain Chem Eng 2018. https://doi.org/10.1021/acssuschemeng.8b01637. in press.
[88] Huang J, Cao Y, Shao Q, Peng X, Guo Z. Magnetic nanocarbon adsorbents with enhanced hexavalent chromium removal: morphology dependence of fibrillar vs particulate structures. Ind Eng Chem Res 2017;56:10689–701.
[89] Gong K, Hu Q, Yao L, et al. Ultrasonic pretreated sludge derived stable magnetic active carbon for Cr(VI) removal from wastewater. ACS Sustain Chem Eng 2018;6:7283–91.
[90] Wang Y, Zhou P, Luo S, et al. Controllable synthesis of monolayer poly(acrylic acid) on channel surface of mesoporous alumina for Pb(II) adsorption. Langmuir 2018;34:7859–68.
[91] Ma Y, Lyu L, Guo Y, et al. Porous lignin based poly (acrylic acid)/organo-montmorillonite nanocomposites: swelling behaviors and rapid removal of Pb (II) ions. Polymer 2017;128:12–23.

[92] Zhang Y, Zhao M, Zhang J, et al. Excellent corrosion protection performance of epoxy composite coatings filled with silane functionalized silicon nitride. J Polym Res 2018;25:130.
[93] Wang C, Wu Y, Li Y, et al. Flame retardant rigid polyurethane foam with a phosphorus-nitrogen single intumescent flame retardant. Polym Adv Technol 2018;29:668–76.
[94] Wu Z, Gao S, Chen L, et al. Electrically insulated epoxy nanocomposites reinforced with synergistic core-shell SiO2@MWCNTs and montmorillonite bifillers. Macromol Chem Phys 2017;218:1700357.
[95] Xu M, Ma K, Jiang D, Zhang J, Zhao M, Guo X, et al. Hexa-[4-(glycidyloxycarbonyl) phenoxy]cyclotriphosphazene chain extender for preparing high-performance flame retardant polyamide 6 composites. Polymer 2018;146:63–72.
[96] Xie P, Wang Z, Zhang Z, Fan R, Cheng C, Liu H, et al. Silica microsphere templated self-assembly of a three-dimensional carbon network with stable radio-frequency negative permittivity and low dielectric loss. J Mater Chem C 2018;6(19):5239.
[97] Gu J, Dong W, Tang Y, et al. Ultra-low dielectric, fluoride-containing cyanate ester resins combining with prominent mechanical properties and excellent thermal and dimension stabilities. J Mater Chem C 2017;5:6929–36.
[98] Song Y, He L, Zhang X, et al. Highly efficient electromagnetic wave absorbing metal-free and carbon-rich ceramics derived from hyperbranched polycarbosilazanes. J Phys Chem C 2017;121:24774–85.
[99] Luo C, Duan W, Yin X, Kong J. Microwave absorbing polymer-derived ceramics from cobalt coordinated poly(dimethylsilylene)diacetylenes. J Phys Chem C 2016;120:18721–32.